Current Biology 24, 1909–1917, August 18, 2014 ©2014 Elsevier Ltd All rights reserved http://dx.doi.org/10.1016/j.cub.2014.07.001

Report

Matrix Elasticity Regulates Lamin-A,C Phosphorylation and Turnover with Feedback to Actomyosin

Amnon Buxboim,[1,2,3] Joe Swift,[1,3] Jerome Irianto,[1] Kyle R. Spinler,[1] P.C. Dave P. Dingal,[1] Avathamsa Athirasala,[1] Yun-Ruei C. Kao,[1] Sangkyun Cho,[1] Takamasa Harada,[1] Jae-Won Shin,[1] and Dennis E. Discher[1,2,*]

[1]Molecular and Cell Biophysics Lab

[2]Physics and Astronomy

University of Pennsylvania, Philadelphia, PA 19104, USA

Summary

Tissue microenvironments are characterized not only in terms of chemical composition but also by collective properties such as stiffness, which influences the contractility of a cell, its adherent morphology, and even differentiation [1–8]. The nucleoskeletal protein lamin-A,C increases with matrix stiffness, confers nuclear mechanical properties, and influences differentiation of mesenchymal stem cells (MSCs), whereas B-type lamins remain relatively constant [9]. Here we show in single-cell analyses that matrix stiffness couples to myosin-II activity to promote lamin-A,C *de*phosphorylation at Ser22, which regulates turnover, lamina physical properties, and actomyosin expression. Lamin-A,C phosphorylation is low in interphase versus dividing cells, and its levels rise with states of nuclear rounding in which myosin-II generates little to no tension. Phosphorylated lamin-A,C localizes to nucleoplasm, and phosphorylation is enriched on lamin-A,C fragments and is suppressed by a cyclin-dependent kinase (CDK) inhibitor. Lamin-A,C knockdown in primary MSCs suppresses transcripts predominantly among actomyosin genes, especially in the serum response factor (SRF) pathway. Levels of myosin-IIA thus parallel levels of lamin-A,C, with phosphosite mutants revealing a key role for phosphoregulation. In modeling the system as a parsimonious gene circuit, we show that tension-dependent stabilization of lamin-A,C and myosin-IIA can suitably couple nuclear and cell morphology downstream of matrix mechanics.

Results and Discussion

Lamin-A,C Phosphorylation in Interphase Cells Is Favored by Low Nuclear Stress

The inner nuclear membrane is lined by juxtaposed networks of two types of intermediate filament proteins. The main products of the *LMNA* gene, lamin-A and the truncated spliceform lamin-C, have long been known to vary greatly between different tissues [10]. *LMNB1* is the founding member of the intermediate filament superfamily [11] that also includes *LMNB2*, which varies minimally in expression between different tissues [9]. The lamina interacts with numerous nuclear proteins and chromatin, as well as links across the nuclear envelope to the cytoskeleton [12–14]. Our recent proteomics analyses of tissue samples and cells showed that lamin-A,C (LMNA) is unique among these various factors in increasing systematically with tissue stiffness [9]. We further showed with cultured cells that lamin-A,C increases with matrix stiffness and can enhance differentiation, although the molecular basis for mechanoregulation was unclear. Mass spectrometry (MS) of bulk lysates suggested that lamin-A,C was more phosphorylated on soft matrices than stiff matrices while B-type lamins showed no detectable phosphorylation. All lamins are abundantly phosphorylated in rounded mitotic cells (uncaging the chromatin). One of the best-characterized phosphorylation sites in lamin-A,C is Ser22 [15, 16], for which there is an antibody suitable for high-resolution cell imaging. We therefore hypothesized that pSer22 in individual interphase cells would be highest in states of low cell tension.

Quantitative immunofluorescence showed pSer22 in the nuclei of every cell (Figure 1A and Figures S1A–S1C available online), amounting to ~5%–10% of total lamin-A,C as calibrated by synthetic peptides using MS (Figures 1B, S1D, and S1E). Intensities in each interphase nucleus were at least several fold above the intensity of the secondary antibody control (Figure S1B) while also being ~10-fold less than those in dividing cells (Figures 1B, S1C, and S1D). Specificity of anti-pSer22 was confirmed with an epitope blocking phosphopeptide that greatly decreased signal in both nondividing nuclei and dividing cell cytoplasm (Figure 1B). Lamin-A,C is thus phosphorylated at Ser22 during interphase. The A549 cell line used in these initial imaging studies possesses some key mesenchymal characteristics [17], but similar observations apply to primary human MSCs that are well known for their contractility-modulated adhesion [2].

Mesenchymal stem cells (MSCs) were seeded from suspension onto soft (0.3 kPa) or stiff (40 kPa) collagen-coated matrices and were then fixed and imaged at various time points. The fraction of lamin-A,C phosphorylated at Ser22 (pSer22/LMNA) decreased concomitantly with greater nuclear spreading and total lamin-A,C, which were both promoted by stiff matrix (Figure 1C). Cells cultured on a very thin layer (3–15 μm) of soft matrix on top of glass exhibited behavior intermediate between that of cells on soft and stiff gels (both >35 μm thick), and indeed in the case of total lamin-A,C and pSer22 per LMNA, the thin, soft gel behaved most like the thick, stiff gel. The thin, soft gel had the same chemical composition as the thicker soft gel, but the proximity of the hard glass substrate increases the apparent stiffness "felt" by the cell so that hydrogel composition seems unimportant [18, 19]. After 24 hr, lamin-A,C dephosphorylation on soft gels was one-half of that on stiff matrices, but changes in phosphorylation were observed within hours of cell adhesion, which is similar in time scale to changes in lamin-A,C level and nuclear spreading. Rapid posttranslational changes under stress have been reported in other mechanotransduction pathways such as p130Cas when extended by cell tension to expose sites for phosphorylation [4] (opposite to the trend here). For lamin-A,C in isolated nuclei, we have recently demonstrated stress modulation of a site-specific, nonenzymatic modification (i.e., fluorophore conjugation to a buried cysteine) [9], and so stress modulation of lamin-A,C phosphorylation could

[3]Co-first author

*Correspondence: discher@seas.upenn.edu

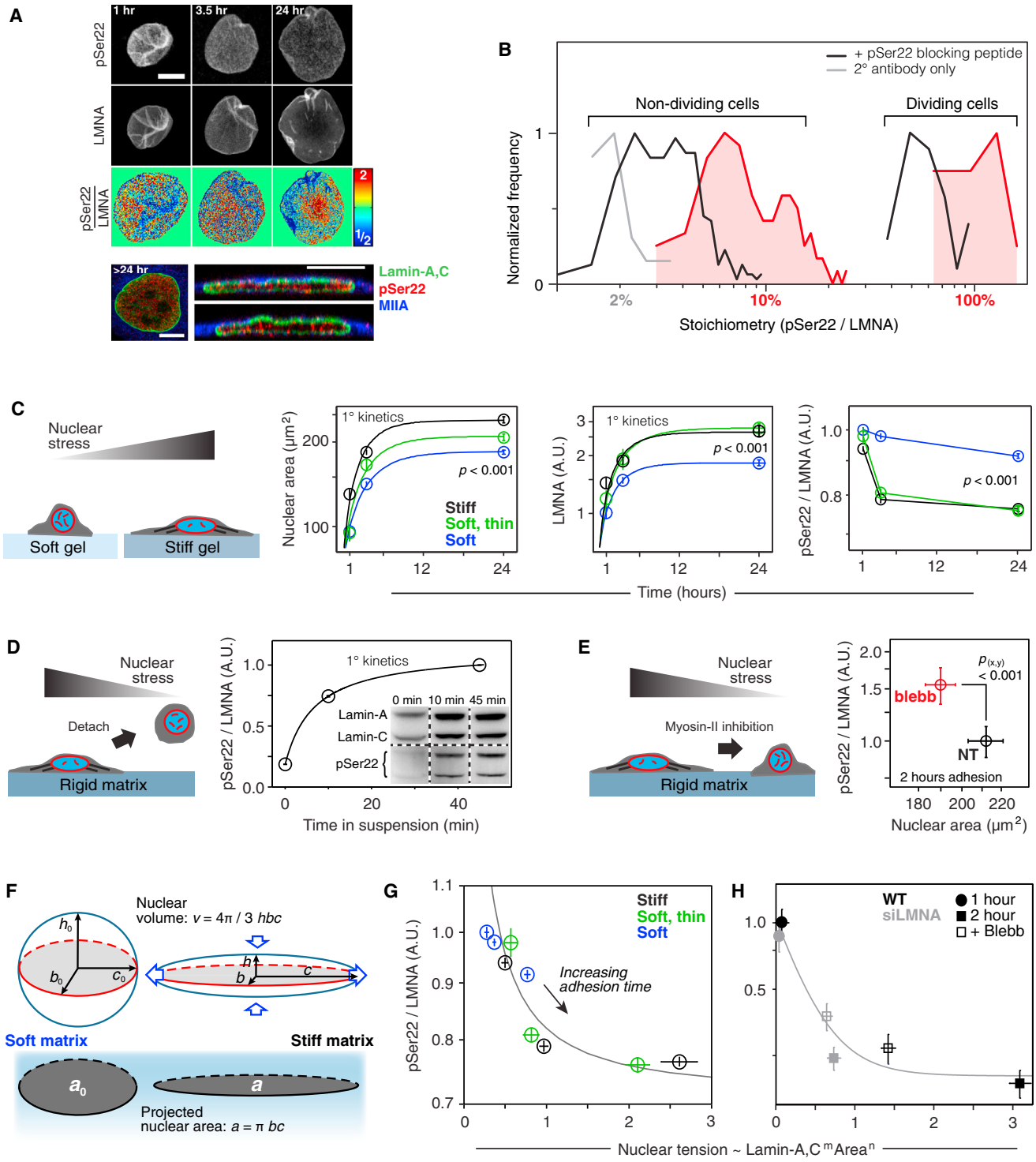

Figure 1. Increased Stress on the Nucleus Suppresses Lamin-A,C Phosphorylation

(A) Lamin-A,C pSer22 is present in interphase cells. As shown in the top two rows, confocal image stacks of total and pSer22 lamin-A,C in MSCs fixed after 1–24 hr of adhesion showed wrinkled nuclei at early stages of cell adhesion that stretched and smoothed with spreading. The third row shows pSer22/LMNA ratios from the top two rows calculated pixel by pixel and normalized to the mean fold change. After 24 hr, a greater phospho-LMNA concentration was observed in the nucleoplasm versus the nuclear periphery. The bottom row shows confocal cross-sections that confirmed nucleoplasmic pSer22. Scale bars, 10 μm.

(B) Histogram of pSer22 levels in a population of A549 cells (Figures S1A–S1D) showing specificity of pSer22 immunofluorescence and stoichiometry calibrated by MS (Figure S1E). Dividing cells showed the greatest extent of phosphorylation (Figure S1C). Preincubation with a phosphoepitope-blocking peptide decreased immunofluorescence intensity, as did nonspecific binding to a nonphosphorylated version of the same peptide, but to a significantly lesser extent (Figure S1D). In the absence of primary antibody (second-degree antibody only), fluorescence intensity was very low. n = 33–249 cells per group.

(legend continued on next page)

likewise depend on stress modulation of lamin-A,C's structure. However, here where we focus on the important downstream consequences of phosphorylated lamin-A,C after providing further evidence of a stress-modulated mechanism.

Upon detachment from substrate into suspension, MSCs and their nuclei rapidly rounded as cytoskeletal tension was relaxed. This process was accompanied within tens of minutes by lamin-A,C phosphorylation at Ser22 (Figure 1D). Cytoskeletal tension was similarly relaxed by treatment with the myosin-II inhibitor blebbistatin (blebb), resulting in a reduction in nuclear spread area and increased pSer22/LMNA (Figures 1E and S1E). Knockdown (KD) of myosin-IIA also increased pSer22/LMNA (Figure S1F), and expression of a phosphomimetic myosin-IIA construct, S1943D, known to suppress stress fiber assembly [20, 21] lowered the amount of lamin-A,C (Figure S1G). Matrix mechanics, cell detachment or reattachment, cell spreading, and myosin inhibition all collectively and independently support the conclusion that low nuclear stress favors lamin-A,C phosphorylation.

A nominal "nuclear tension" in cell spreading was estimated from the product of nuclear strain and nuclear stiffness, as calculated respectively from the fold change in projected nuclear area (Figure 1F) and from the level of lamin-A,C, which contributes to stiffness (see the Supplemental Information). Replotting of the pSer22/LMNA values for matrix-dependent MSC spreading (Figure 1C) and blebb treatment (Figure 1E) versus nuclear tension collapsed all of the data onto hyperbolic decays, consistent with inhibition of lamin-A,C phosphorylation by nuclear tension (Figures 1G and 1H).

Lamin-A Phosphomutants Moderate Nuclear Mechanosensitivity

For assessment of the functional importance and properties of lamin-A,C phosphorylation, MSCs were transfected with GFP fusions of lamin-A having either a phosphomimetic S22D or a nonphosphorylatable S22A and compared to cells transfected with WT GFP-lamin-A. Fluorescence recovery after photobleaching (FRAP; Figure 2A) was used to assess the mobile fractions, *f*, (at 5–10 min) of the S22 variant proteins during and after cell attachment to soft and stiff substrates. FRAP was started 30 min after plating of MSCs, and blebb was added after 24 hr. Up to 30%–40% of WT GFP-lamin-A was mobile 30 min after plating, regardless of matrix stiffness (Figure S2A). However, lamin-A was progressively immobilized with cell adhesion, and by just 2 hr (with $\tau \approx 1$ hr) the soluble fraction was a stable ~15% on soft matrix and <5% on stiff matrix. The higher mobility of WT GFP-lamin-A in rounded nuclei on soft matrix at both 2 hr and 24 hr, and also after inhibition of contractility with blebb treatment (Figure 2B), was consistent with higher pSer22 (Figures 1C and 1E). These findings are also consistent with the fact that during cell division the phosphorylation of Ser22 solubilizes lamin-A,C [15].

In contrast to WT lamin-A, neither S22D nor S22A exhibited a dependence of the mobile fraction, *f*, on matrix stiffness (Figures 2B and S2B). Phosphorylation of lamin-A thus appeared to be downstream of matrix. Moreover, S22D mobility remained high 4-fold longer than the WT ($\tau \approx 4$ hr), regardless of stiffness. Although by 24 hr *f* was similar for S22D and the WT on soft gels, perhaps due to phosphorylation of sites other than Ser22, blebb had no significant effect on *f* for S22D. Since S22A lamin-A was completely immobilized after only 2 hr of adhesion to any matrix (Figure S2B), the phosphodynamics of Ser22 seemed important to lamin-A,C mobility. A similar increase in mobile fraction for phosphomimetic S22E lamin-A over the WT and S22A was observed in lung carcinoma A549 cells (Figure S2C).

While ectopically expressed WT GFP-LMNA localized predominantly at the nuclear envelope, as did S22A, the phosphomimetic S22D appeared to be more homogenous within MSC nuclei (Figure 2C). A diffuse nuclear distribution of S22D was consistent with confocal z stack imaging that showed nucleoplasmic pSer22 staining in fixed MSCs (Figure 1A, bottom). Live-cell imaging showed that both S22D and S22A completely suppressed differences in nuclear area between cells on soft and stiff matrices: while the WT-expressing cells had twice the nuclear area on stiff versus soft matrix, S22D suppressed nuclear spreading on stiff matrix and S22A suppressed nuclear rounding on soft matrix (Figure 2D). The morphological and molecular-structural characteristics of S22 phosphomutants were also accompanied by significant changes in nuclear deformability (Figure 2E): the relaxation times of micropipette-aspirated nuclei at fixed stress showed softening of S22D nuclei and stiffening with S22A relative to the WT. The phosphodynamics of S22 in lamin-A,C are thus critical in determining the structural organization and mechanics of nuclei during cell spreading.

Lamin-A,C Degradation Is Downstream of Phosphorylation

During cell division, comprehensive phosphorylation is required to disassemble the lamina, but during interphase, our results suggest that cells titrate lamin-A,C levels and phosphorylation to regulate molecular mobility and nuclear stiffness in proportion to cytoskeletal stress and matrix stiffness. We hypothesized that these processes were linked, with high pSer22 in relaxed cells favoring lamin-A,C degradation.

(C) Stiff matrix enhances nuclear stress which inhibits phosphorylation of lamin-A,C. Stress on nuclei in MSCs was manipulated by changing of matrix stiffness and adhesion time. Cells spread, with correspondingly greater projected nuclear areas, with increasing adhesion time and to a greater extent on stiff (40 kPa, black line) versus soft (0.3 kPa, blue line) substrate. A thin, soft matrix (0.3 kPa, green line) showed behavior intermediate between soft and stiff. The matrix-modulated adhesion process was accompanied by an increase in the total LMNA and a reduction in the fraction of pSer22/LMNA. Error bars in all plots show ±SEM. n = 77–276 cells per group.

(D) Cell detachment increased pSer22/LMNA in rounding nuclei, with phosphorylation (quantified by immunoblot; n = 3) increasing over tens of minutes in suspension, consistent with relaxation of nuclear stress.

(E) pSer22/LMNA increased with myosin-IIA inhibition and stress relaxation by blebbistatin (blebb) treatment (immunofluorescence, Figure S1E). n = 25–32 cells per group.

(F) Nuclear shape was modeled as an ellipsoid, with surface area assumed to be constant during nuclear deformation. During cell spreading, the nucleus was stretched and flattened down against the substrate, subject to tangential stretching ("hoop strain") but negligible radial strain. As the hoop strain scaled with the radius, *r*, and the fold change in *r* can be estimated by the square root of the fold change in projected nuclear area, we concluded that the nuclear strain involved in cell spreading can be estimated by $\varepsilon \sim \sqrt{a/a_0}$, where *a* is the nuclear projected area and a_0 corresponds to the initial state.

(G) Via expression of nuclear tension as a function of lamin-A,C level and nuclear area, pSer22/LMNA data were fit to hyperbolic decays. The plot shows data fitting for MSCs cultured on hydrogel substrates that are soft, or soft and thin, or stiff (adhesion time: 1, 3.5, and 24 hr; Figure 1C).

(H) Data fitting for MSCs subjected to lamin-A,C KD and blebb treatment (Figures 1E and S1E).

Error bars indicate ±SEM. See also Figure S1.

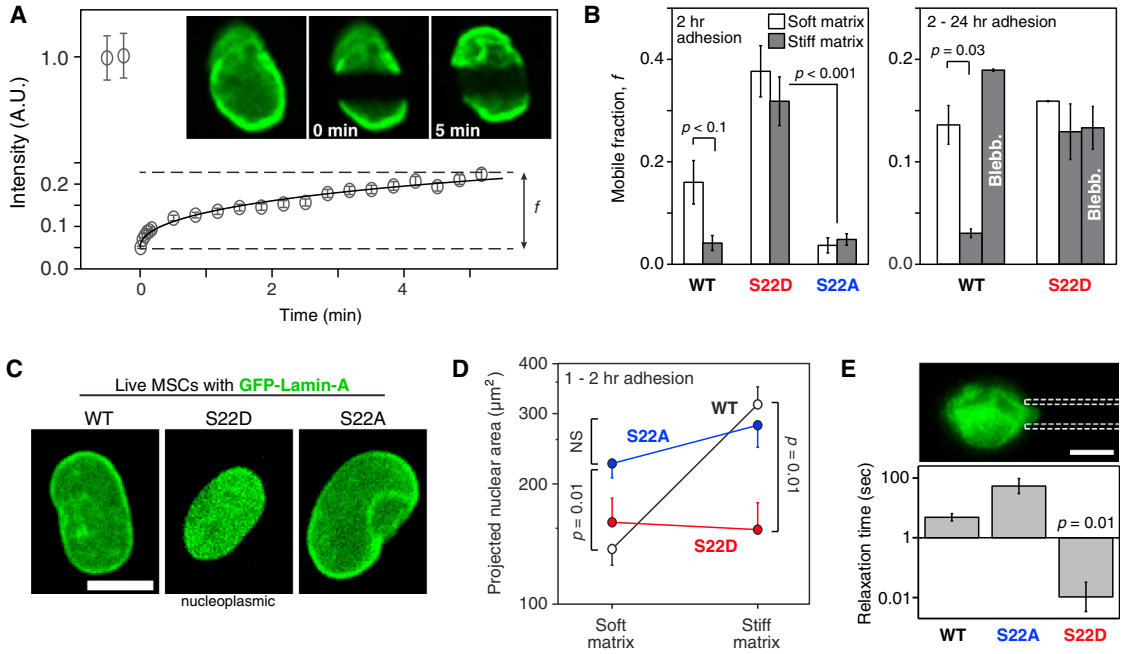

Figure 2. Phosphomimetic Lamin-A Constructs Show Increased Mobility and Soften the Nucleus

(A) The mobile fraction, *f*, of GFP-fused wild-type lamin-A and phosphomutant lamin-A constructs (S22D and S22A) was evaluated by fitting of an exponential curve to the recovering intensities of wide side-to-side bands photobleached in the nuclei of MSCs.

(B) Analysis of FRAP experiments showed that the WT construct was comparatively more mobile in MSCs cultured for 2 hr on soft (0.3 kPa) than on stiff (40 kPa) substrate (Figure S2A). Independent of matrix stiffness, S22D mobile fractions were higher than the WT, whereas S22A remained polymerized (Figure S2B). WT lamin-A was solubilized by blebb after 24 hr on stiff gels, but treatment of phosphomimetic S22D showed no significant change. n = 9–18 nuclei per group.

(C) Live-cell imaging of WT, S22D, and S22A phosphomimetic GFP-lamin-A constructs. S22D showed a diffusive nucleoplasmic distribution and low nuclear spreading, consistent with a nucleoplasmic distribution of pSer22.

(D) S22D and S22A suppressed matrix mechanosensitivity of MSCs, whereas WT nuclei spread by >2-fold on stiff matrix (40 kPa) relative to soft matrix (0.3 kPa). n = 5–18 nuclei per group.

(E) Relaxation times measured by micropipette aspiration showed S22D nuclei to be significantly softer than WT nuclei, and S22A nuclei were moderately stiffer. Relaxation times were determined at the same value of creep compliance ($J = 1.4\ kPa^{-1}$) per [22]. Error bars show the log mean ± SEM. n > 4 nuclei. Error bars indicate ±SEM. See also Figure S2.

Full-lane immunoblots of lamin-A,C in MSCs maintained in suspension in serum-supplemented media for 10 or 45 min showed a decrease in intact lamin-A,C with time and slightly increased intensity of weak lower bands (Figure 3A). Immunostaining of the same blots for pSer22 revealed the same bands plus many additional lower bands, with densitometry illustrating the differences (Figures 3B, S3A, and S3B). So that specificity of the antibody could be confirmed, gels were sliced for MS analyses, and the lower-molecular-weight (MW) bands indeed yielded up to 28 distinct lamin-A,C-derived peptides (Figures 3C, 3D, and S3C). Lamin-A,C peptides were found in each of the lower-MW gel slices from lysates of MSCs and A549 cells (Figures 3D and S3D). Immunoblotting with antibody against cleaved lamin-A also revealed an abundance of signal at low MW with very little signal from intact protein (Figure 3E). Immunoblot analyses—as with any bulk technique—could reflect distinct subpopulations of cells, but immunofluorescence imaging demonstrated that anti-pSer22, as well as monoclonal and polyclonal antibodies against anti-cleaved lamin-A, produced significant signal in every nucleus (Figure S3F).

To assess whether degradation could be downstream of phosphorylation, we leveraged the fact that lamin-A,C is classically a target of cyclin-dependent kinases (CDKs). MSCs were treated with an inhibitor, RO3306, shown to act against several CDKs at μM concentration [23]; treatments of ≤6 hr tend to minimize extraneous changes in protein levels. In drug-treated cells, quantitative immunofluorescence revealed a ~50% decrease in pSer22 and >80% decrease in immunostaining of cleaved lamin-A,C, as assessed with two independent antibodies (Figures 3F, 3G, and S3F). Drug-treated cells also showed higher lamin-A,C and larger nuclear areas, consistent with a high-contractility phenotype induced by phosphoinhibition (Figure S3G). Additionally, plotting of pSer22/LMNA as a function of nuclear tension (as in Figures 1G and 1H) fit to an appropriate hyperbolic form (Figure S3H). Since the CDK inhibitor suppressed lamin-A,C phosphorylation and degradation, we expected that drug-treated nuclei would also be stiffer in micropipette aspiration; indeed, the nuclear relaxation times were ~10,000-fold longer than untreated cells (Figure 3H). Phosphorylation of lamin-A,C thus precedes turnover and nuclear softening.

Correlated Phosphorylation of S390 and S22 Sites in Lamin-A,C

A large number of lamin-A,C phosphorylation sites have been identified by MS, with many occurring in mitosis [24–26]. Our earlier MS studies identified Ser22, Ser390, Ser404, and Thr424 as more phosphorylated on soft compared to stiff substrate [9], and recent work has associated phosphorylation of

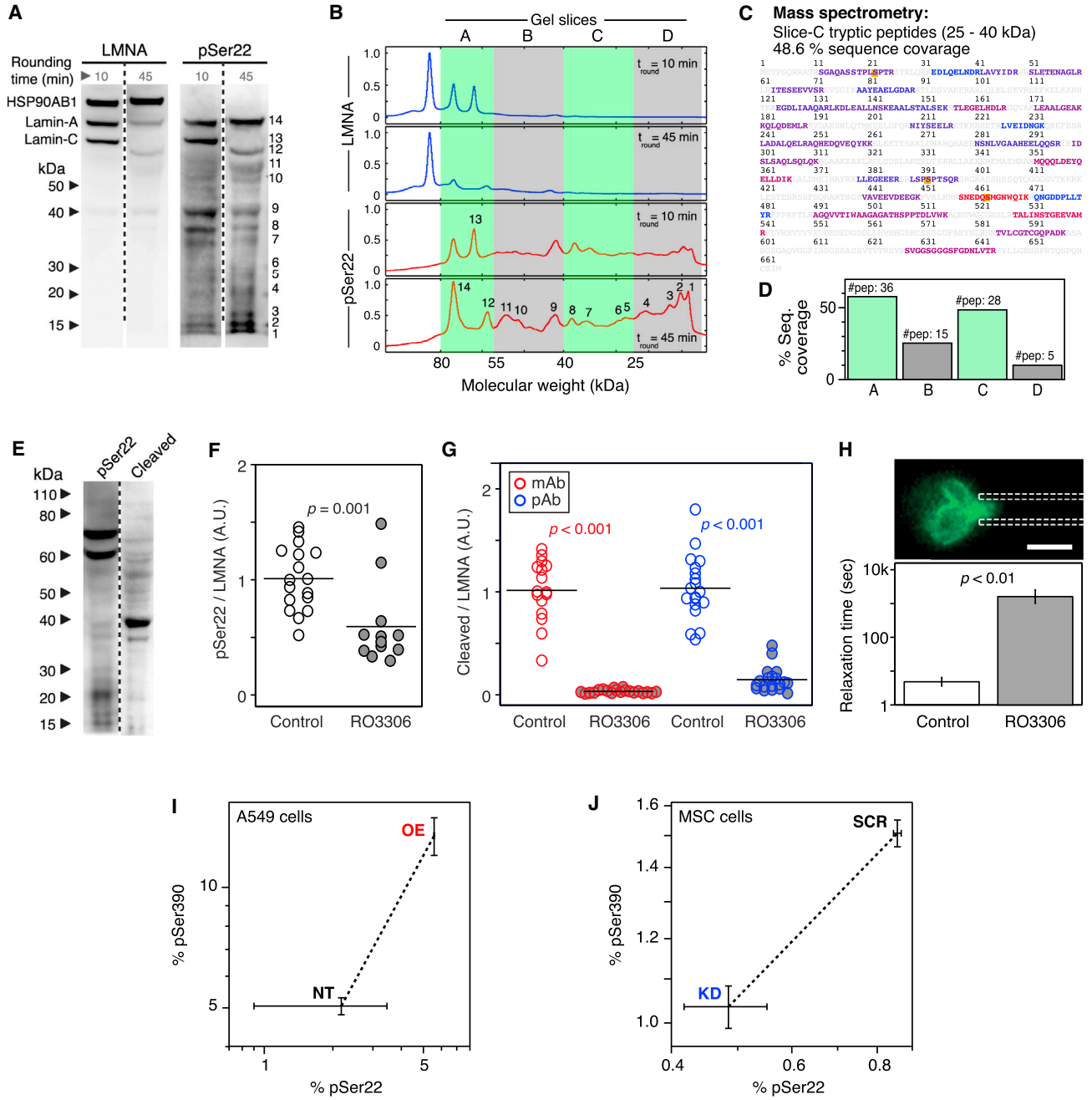

Figure 3. Phosphorylation of Lamin-A,C Promotes Proteolysis and Nuclear Softening

(A) Phospho-lamin-A,C is present in both full-length and cleaved states. MSCs lysed after short (10 min) and long (45 min) periods of rounding in suspension showed numerous low-MW, fragmentation-product bands in immunoblots against lamin-A,C and, to a greater extent, against pSer22.

(B) Profiles of immunoblots showing MW ranges analyzed by MS (densitometry shown in Figures S3A and S3B).

(C) Gel slices A–D were analyzed by MS, confirming the existence of low-MW lamin-A cleavage products (peptide coverage of 25–40 kDa range is shown; blue-to-red coloring indicates peptides detected with increased ion current). Phosphorylation sites detectable by MS are indicated in yellow.

(D) All examined bands had lamin-A fragments (see Figure S3C for sequence coverage maps).

(E) Inhibition of lamin-A,C phosphorylation suppresses cleavage. Immunoblots against lamin-A pSer22 or lamin-A cleavage product(s) are shown. The latter antibody shows minimal detection of intact lamin-A and a high-intensity band at 40 kDa.

(F) Treatment with CDK inhibitor RO3306 reduced the extent of phosphorylation at Ser22 in MSCs.

(G) RO3306 also suppressed the formation of lamin-A,C cleavage products as determined by two independent antibodies (see Figures S3F–S3H for representative images and analysis).

(H) Drug-induced lamin-A,C phosphoinhibition stiffened the nucleus as determined by micropipette aspiration (relaxation times determined at constant compliance, $J = 1.25\ kPa^{-1}$ per [22]). Error bars show the log mean ± SEM. n > 4 nuclei.

(I) MS showed a correlated increase in phosphorylation at S22 and S390 during lamin-A overexpression in A549 cells.

(J) Phosphorylation at S22 and S390 showed a correlated decrease during lamin-A,C KD in MSCs. Error bars show ±SEM. (See Figure S1D for calibration of phosphorylation measurements by MS.)

Error bars indicate ±SEM. See also Figure S3.

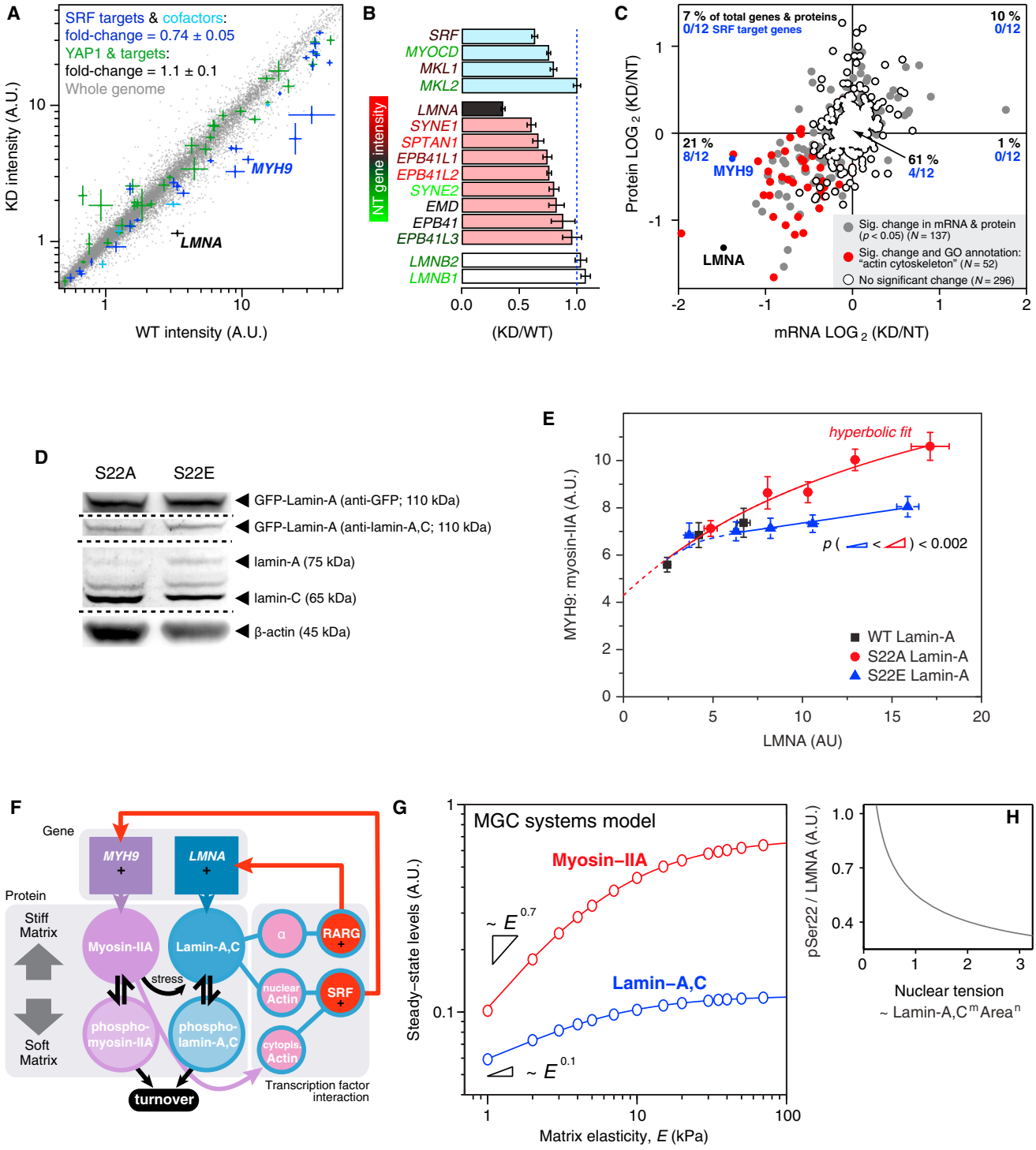

Figure 4. Lamin-A,C Level and Phosphorylation State Regulate Myosin-IIA, Factors that Can Be Combined into a Mechanosensitive Gene Circuit Model

(A) Lamin-A,C level regulates myosin-IIA through the serum response factor (SRF) pathway. Transcriptional profiling of MSCs subjected to lamin-A,C KD is shown (n = 3) versus nontreated wild-type control (NT or WT, equivalent). SRF and cofactors (in cyan) and target genes (blue) were significantly suppressed. The YAP1-regulated Hippo pathway has also been implicated in cellular mechanosensitivity [7], but it appeared to be unaffected here.

(B) Transcripts of SRF and cofactors (cyan) were suppressed with lamin-A,C KD, along with those of multiple actin-binding nuclear envelope proteins (red) (n = 3). (See Figure S4A for Gene Ontology term analysis.)

(C) Correlation between protein and transcript changes with lamin-A,C KD in MSCs. Points represent 485 proteins quantified by MS with three or more peptides per protein, and their associated mRNA was quantified by DNA microarray. Each point is averaged from three biological replicates, and the transcripts or proteins that are significantly perturbed ($p < 0.05$) are counted in the four quadrants of the plot. Of genes with Gene Ontology annotation "actin cytoskeleton," (n = 52, in red), 14 are unchanged and 36 have reduced levels of protein and mRNA. Of genes classified as SRF targets (n = 12) by Olson et al., four are unchanged and eight—including myosin-IIA (*MYH9*)—have reduced levels of protein and mRNA [31].

(legend continued on next page)

Ser404 with turnover of lamin-A precursor [27]. While the well-studied pSer22 modification is recognized by commercial antibodies, MS analyses of multiple samples showed that overexpression of lamin-A resulted in greater phosphorylation of both Ser22 and Ser390 (Figure 3I). The addition here of excess lamin-A, perturbing the mechanical equilibrium of the cell and conceivably relieving or disrupting tension on the nucleoskeleton, is perhaps compensated for in the cell by increased phosphorylation and subsequent lamin turnover. Conversely, lamin-A,C KD resulted in reduced phosphorylation at both sites, thus helping to maintain the integrity of the diminished lamina (Figure 3J). Furthermore, titration with synthetic peptides showed Ser390 to be phosphorylated 1%–5% in both A549 cells and MSCs (Figure S1E). Importantly, the same pSer390 phoshopeptide was also detected in tryptic peptides from lysates of multiple mouse tissues (brain, muscle, and heart) [9], but the numerous cell types in such tissues complicate interpretations and strongly motivate the studies of specific human cell types here.

Lamin-A,C Level and Phosphomutants Regulate Myosin-IIA

Since the phosphomimetic mutant of lamin-A,C led to nuclear rounding and lamin-A,C interacts with nuclear actin and actin-binding proteins [28, 29] to partially regulate at least a few components in the serum response factor (SRF) pathway [9, 30], we hypothesized broad control of actomyosin gene expression [31]. Whole-genome transcriptional profiling of *LMNA* KD MSCs showed repression of target genes and cofactors of the mechanosensitive SRF pathway (Figures 4A and 4B), leading to broad suppression of the actin cytoskeleton to a greater extent than in any other pathways (Figure S4A). Proteomic profiles showed excellent correlation with transcript profiles, with all significantly altered SRF targets, including myosin-IIA (*MYH9* gene), being repressed at both the protein and mRNA level (Figure 4C).

To investigate a functional link between lamin-A,C phosphorylation and myosin-IIA (MYH9), we established A549 cell lines with small hairpin RNA knockdown of endogenous lamin-A,C plus transduction with GFP-lamin-A constructs WT, S22E, and S22A (Figures 4D and S4B–S4D). The phosphomimetic showed in the immunoblot a lower-MW band consistent with Figure 3E and phosphorylation-initiated degradation. Overexpression of lamin-A generally increased myosin-IIA above a basal level (Figure 4E), and at higher overexpression levels of the nonphosphorylatable and immobile S22A construct, myosin-IIA increased to a much greater extent compared to overexpression of phosphomimetic S22E. A hyperbolic fit to the S22A data intercepted the y axis at a nonzero value, suggesting that a fraction of myosin-IIA expression is independent of lamin-A,C, which is consistent with the presence of this essential myosin in lamin-A,C knockout mice [32, 33]. Since lamin-A,C primarily regulates the actomyosin cytoskeleton, depolymerization of F-actin in our studies of nuclear stiffness (see the Experimental Procedures) as modulated by lamin-A,C phosphorylation (Figures 2E and 3H) seems likely to reveal properties attributable directly to the structural state of lamin-A,C.

Systems Mechanobiology Gene Circuit Couples Lamin-A,C and Myosin-IIA Expression

While our recent work established that lamin-A,C positively regulated its own transcription factor [9], lamin-A,C phosphodynamics here affect also myosin-IIA levels. Based on these and additional experimental insights, a parsimonious model of expression and degradation for both lamin-A,C and myosin-IIA message and protein was formulated as a "mechanobiological gene circuit" (MGC) (Figure 4F and the Supplemental Information) in order to assess whether a stably coupled system could be reasonably achieved. The most important and atypical aspect of the model is mechanically regulated degradation of these two structural proteins, which follows otherwise standard cooperative Michaelis-Menten-type enzyme kinetics. Transcription of both genes was assumed to be linear in lamin-A,C protein, and linearity was also assumed for degradation of transcript as well as for protein synthesis. Equations describing the MGC were solved numerically, constrained by experimental observations (Figures 1G and 1H and the Supplemental Information), and the nonlinear degradation terms fed back into the gene circuit to generate stable expression states of both lamin-A,C and myosin-IIA (Figure 4G). As matrix stiffness and cell tension suppressed protein phosphorylation and turnover (modeled from relations in the MGC in Figure 4H), steady-state levels monotonically increased with matrix *E*, consistent with coupled mechanoregulation of lamin-A,C and myosin-IIA. With this initial model in hand, further experiments will be needed to measure the stress-dependent rate constants for the lamins and many other relevant proteins. Next-generation, high-throughput methods of sequencing and proteomics seem highly appropriate [34] for these microenvironment-dependent metabolic questions.

Experimental Procedures

Additional details of the isolation and culture of primary MSCs, cell treatments and phosphomimetic constructs, immunofluorescence and confocal imaging, FRAP, immunoblotting, transcriptional profiling, and

(D) S22A and E GFP-lamin mutants expressed in cells with knockdown of endogenous lamin-A,C show roughly similar levels of both constructs and endogenous protein.

(E) Lamin-A,C phosphorylation feeds back into myosin-IIA level. Expression of increasing levels of phosphomimetic GFP-S22E-lamin-A in A549 cells with KD of endogenous lamin-A,C had minimal effect on myosin-IIA levels. In contrast, expression of an nonphosphorylatable S22A construct caused a relatively increased quantity of myosin-IIA [the x axis shows total LMNA; S22A data were fit by the hyperbolic function $y = abx\ (1 + bx)^{-1} + c$ (a = 1.3; b = 5.5; c = 4.3; $R^2 > 0.95$); each point is averaged data from n > 20 cells; see Figures S4B–S4D for representative images and analysis of cell morphology].

(F) Tension-dependent phosphorylation and turnover feeds into transcriptional regulation, as captured by a mechanobiological gene circuit (MGC) systems model that couples both lamin-A,C and myosin-IIA levels to matrix stiffness. Lamin-A,C transcriptionally regulates *LMNA* via the retinoic acid pathway (through a mediator, α) and also *MYH9* via the SRF pathway through nuclear actin. On stiff matrix, nonphosphorylated, contraction-competent myosins positively regulate lamin-A,C, favoring assembly and opposing degradation that occurs on soft matrices.

(G) The MGC systems model predicted that lamin-A,C and myosin-IIA levels should monotonically increase with matrix elasticity but also saturate on rigid substrates.

(H) MGC model suggests decreased lamin phosphorylation with increasing nuclear tension (consistent with the model and experimental data shown in Figures 1F–1H).

Error bars indicate ±SEM. See also Figure S4.

micropipette aspiration can be found in the Supplemental Experimental Procedures.

Preparation of Soft and Stiff Hydrogel Substrates

The preparation of polyacrylamide gels with controlled elasticity and covalent attachment to glass coverslips was described in detail in a published methods paper [18]; the method is also summarized in the Supplemental Experimental Procedures.

MS and Quantification of Synthetic Phosphopeptides

Quantification of proteins by label-free MS is described in the Supplemental Experimental Proceduresand earlier work [35]. MS response to phosphorylation at S22 and S390 was calibrated using synthetic versions of tryptic peptides (SGAQASSTPLSPTR, SGAQASSTPL[pSer22]PTR, and LRLSP SPTSQR LRL[pSer390]PSPTSQR; GenScript), which were spiked into a tryptic cell digests (60–80 kDa MW band) (Figure S1E). The data in Figures 3C, 3D, and S3C–S3E were attained without alignment between spectra (Elucidator, Rosetta Biosystems). The data in Figures 3I and 3J were aligned against standards containing both phosphorylated and unphosphorylated versions of the S22 and S390 tryptic peptides. Specificity of primary lamin-A pSer22 antibody (rabbit polyclonal, Cell Signaling) was tested by incubation overnight at 4°C in 3% BSA with the corresponding phosphopeptide (SGAQASSTPL[pSer22]PTR) at a peptide:antibody ratio of 10:1 (Figures 1B and S1D).

Systems Mechanobiology Gene Circuit

Derivations of the equations used to describe the interactions in Figure 4F are shown in the Supplemental Information and are solved in the steady state to produce the data plotted in Figures 4G and 4H using code written in Mathematica (Wolfram).

Supplemental Information

Supplemental Information includes Supplemental Experimental Procedures and four figures and can be found with this article online at http://dx.doi.org/10.1016/j.cub.2014.07.001.

Author Contributions

A.B., J.S., J.I., K.R.S., P.C.D.P.D., A.A., Y.C.K., S.C., T.H., and J.S. performed experiments. A.B., J.S., J.I., and D.E.D. organized and wrote the manuscript.

Acknowledgments

We are grateful for support from the US NIH (grants R01HL062352, P01DK032094, R01EB007049, P30DK090969, and NCATS-8UL1TR000003), the US National Science Foundation (grant 1200834), an American Heart Association Grant in Aid (14GRNT20490285), the Human Frontier Science Program, and the University of Pennsylvania's research centers (Materials Research Science and Engineering; Nano Science and Engineering; Nano/Bio Interface).

Received: April 15, 2014
Revised: May 28, 2014
Accepted: July 1, 2014
Published: August 7, 2014

References

1. Discher, D.E., Janmey, P., and Wang, Y.L. (2005). Tissue cells feel and respond to the stiffness of their substrate. Science *310*, 1139–1143.
2. Engler, A.J., Sen, S., Sweeney, H.L., and Discher, D.E. (2006). Matrix elasticity directs stem cell lineage specification. Cell *126*, 677–689.
3. Levental, K.R., Yu, H., Kass, L., Lakins, J.N., Egeblad, M., Erler, J.T., Fong, S.F.T., Csiszar, K., Giaccia, A., Weninger, W., et al. (2009). Matrix crosslinking forces tumor progression by enhancing integrin signaling. Cell *139*, 891–906.
4. Sawada, Y., Tamada, M., Dubin-Thaler, B.J., Cherniavskaya, O., Sakai, R., Tanaka, S., and Sheetz, M.P. (2006). Force sensing by mechanical extension of the Src family kinase substrate p130Cas. Cell *127*, 1015–1026.
5. Even-Ram, S., Doyle, A.D., Conti, M.A., Matsumoto, K., Adelstein, R.S., and Yamada, K.M. (2007). Myosin IIA regulates cell motility and actomyosin-microtubule crosstalk. Nat. Cell Biol. *9*, 299–309.
6. Gardel, M.L., Schneider, I.C., Aratyn-Schaus, Y., and Waterman, C.M. (2010). Mechanical integration of actin and adhesion dynamics in cell migration. Annu. Rev. Cell Dev. Biol. *26*, 315–333.
7. Dupont, S., Morsut, L., Aragona, M., Enzo, E., Giulitti, S., Cordenonsi, M., Zanconato, F., Le Digabel, J., Forcato, M., Bicciato, S., et al. (2011). Role of YAP/TAZ in mechanotransduction. Nature *474*, 179–183.
8. Pelham, R.J., Jr., and Wang, Yl. (1997). Cell locomotion and focal adhesions are regulated by substrate flexibility. Proc. Natl. Acad. Sci. USA *94*, 13661–13665.
9. Swift, J., Ivanovska, I.L., Buxboim, A., Harada, T., Dingal, P.C.D.P., Pinter, J., Pajerowski, J.D., Spinler, K.R., Shin, J.-W., Tewari, M., et al. (2013). Nuclear lamin-A scales with tissue stiffness and enhances matrix-directed differentiation. Science *341*, 1240104.
10. Lehner, C.F., Stick, R., Eppenberger, H.M., and Nigg, E.A. (1987). Differential expression of nuclear lamin proteins during chicken development. J. Cell Biol. *105*, 577–587.
11. Dittmer, T.A., and Misteli, T. (2011). The lamin protein family. Genome Biol. *12*, 222.
12. Schirmer, E.C., Florens, L., Guan, T.L., Yates, J.R., 3rd, and Gerace, L. (2003). Nuclear membrane proteins with potential disease links found by subtractive proteomics. Science *301*, 1380–1382.
13. Gruenbaum, Y., Margalit, A., Goldman, R.D., Shumaker, D.K., and Wilson, K.L. (2005). The nuclear lamina comes of age. Nat. Rev. Mol. Cell Biol. *6*, 21–31.
14. Goldman, R.D., Gruenbaum, Y., Moir, R.D., Shumaker, D.K., and Spann, T.P. (2002). Nuclear lamins: building blocks of nuclear architecture. Genes Dev. *16*, 533–547.
15. Heald, R., and McKeon, F. (1990). Mutations of phosphorylation sites in lamin A that prevent nuclear lamina disassembly in mitosis. Cell *61*, 579–589.
16. Ward, G.E., and Kirschner, M.W. (1990). Identification of cell cycle-regulated phosphorylation sites on nuclear lamin C. Cell *61*, 561–577.
17. Harada, T., Swift, J., Irianto, J., Shin, J.W., Spinler, K.R., Athirasala, A., Diegmiller, R., Dingal, P.C., Ivanovska, I.L., and Discher, D.E. (2014). Nuclear lamin stiffness is a barrier to 3D migration, but softness can limit survival. J. Cell Biol. *204*, 669–682.
18. Buxboim, A., Rajagopal, K., Brown, A.E.X., and Discher, D.E. (2010). How deeply cells feel: methods for thin gels. J. Phys. Condens. Matter *22*, 194116.
19. Buxboim, A., Ivanovska, I.L., and Discher, D.E. (2010). Matrix elasticity, cytoskeletal forces and physics of the nucleus: how deeply do cells 'feel' outside and in? J. Cell Sci. *123*, 297–308.
20. Vicente-Manzanares, M., Ma, X.F., Adelstein, R.S., and Horwitz, A.R. (2009). Non-muscle myosin II takes centre stage in cell adhesion and migration. Nat. Rev. Mol. Cell Biol. *10*, 778–790.
21. Raab, M., Swift, J., Dingal, P.C.D.P., Shah, P., Shin, J.-W., and Discher, D.E. (2012). Crawling from soft to stiff matrix polarizes the cytoskeleton and phosphoregulates myosin-II heavy chain. J. Cell Biol. *199*, 669–683.
22. Dahl, K.N., Engler, A.J., Pajerowski, J.D., and Discher, D.E. (2005). Power-law rheology of isolated nuclei with deformation mapping of nuclear substructures. Biophys. J. *89*, 2855–2864.
23. Vassilev, L.T., Tovar, C., Chen, S.Q., Knezevic, D., Zhao, X.L., Sun, H.M., Heimbrook, D.C., and Chen, L. (2006). Selective small-molecule inhibitor reveals critical mitotic functions of human CDK1. Proc. Natl. Acad. Sci. USA *103*, 10660–10665.
24. Beausoleil, S.A., Villén, J., Gerber, S.A., Rush, J., and Gygi, S.P. (2006). A probability-based approach for high-throughput protein phosphorylation analysis and site localization. Nat. Biotechnol. *24*, 1285–1292.
25. Dephoure, N., Zhou, C., Villén, J., Beausoleil, S.A., Bakalarski, C.E., Elledge, S.J., and Gygi, S.P. (2008). A quantitative atlas of mitotic phosphorylation. Proc. Natl. Acad. Sci. USA *105*, 10762–10767.
26. Olsen, J.V., Vermeulen, M., Santamaria, A., Kumar, C., Miller, M.L., Jensen, L.J., Gnad, F., Cox, J., Jensen, T.S., Nigg, E.A., et al. (2010). Quantitative phosphoproteomics reveals widespread full phosphorylation site occupancy during mitosis. Sci. Signal. *3*, ra3.
27. Bertacchini, J., Beretti, F., Cenni, V., Guida, M., Gibellini, F., Mediani, L., Marin, O., Maraldi, N.M., de Pol, A., Lattanzi, G., et al. (2013). The protein kinase Akt/PKB regulates both prelamin A degradation and Lmna gene expression. FASEB J. *27*, 2145–2155.

28. Zastrow, M.S., Vlcek, S., and Wilson, K.L. (2004). Proteins that bind A-type lamins: integrating isolated clues. J. Cell Sci. *117*, 979–987.
29. Holaska, J.M., Kowalski, A.K., and Wilson, K.L. (2004). Emerin caps the pointed end of actin filaments: evidence for an actin cortical network at the nuclear inner membrane. PLoS Biol. *2*, E231.
30. Ho, C.Y., Jaalouk, D.E., Vartiainen, M.K., and Lammerding, J. (2013). Lamin A/C and emerin regulate MKL1-SRF activity by modulating actin dynamics. Nature *497*, 507–511.
31. Olson, E.N., and Nordheim, A. (2010). Linking actin dynamics and gene transcription to drive cellular motile functions. Nat. Rev. Mol. Cell Biol. *11*, 353–365.
32. Sullivan, T., Escalante-Alcalde, D., Bhatt, H., Anver, M., Bhat, N., Nagashima, K., Stewart, C.L., and Burke, B. (1999). Loss of A-type lamin expression compromises nuclear envelope integrity leading to muscular dystrophy. J. Cell Biol. *147*, 913–920.
33. Kubben, N., Voncken, J.W., Konings, G., van Weeghel, M., van den Hoogenhof, M.M.G., Gijbels, M., van Erk, A., Schoonderwoerd, K., van den Bosch, B., Dahlmans, V., et al. (2011). Post-natal myogenic and adipogenic developmental: defects and metabolic impairment upon loss of A-type lamins. Nucleus *2*, 195–207.
34. Schwanhäusser, B., Busse, D., Li, N., Dittmar, G., Schuchhardt, J., Wolf, J., Chen, W., and Selbach, M. (2011). Global quantification of mammalian gene expression control. Nature *473*, 337–342.
35. Swift, J., Harada, T., Buxboim, A., Shin, J.-W., Tang, H.-Y., Speicher, D.W., and Discher, D.E. (2013). Label-free mass spectrometry exploits dozens of detected peptides to quantify lamins in wildtype and knockdown cells. Nucleus *4*, 450–459.